January 1986 LRP 271/85

COMPUTATION OF MHD EQUILIBRIA BY A QUASI-INVERSE FINITE HYBRID ELEMENT APPROACH

R. Gruber, R. Iacono and F. Troyon

Submitted for publication to J. of Computational Physics

COMPUTATION OF MHD EQUILIBRIA BY A QUASI-INVERSE FINITE HYBRID ELEMENT APPROACH

R. Gruber, R. Iacono and F. Troyon

Centre de Recherches en Physique des Plasmas
Association Euratom - Confédération Suisse
Ecole Polytechnique Fédérale de Lausanne
21, av. des Bains, CH-1007 Lausanne/Switzerland

Abstract

To supply a precise and consistent solution of the Grad-Schlüter-Shafranov equation to the ideal linear MHD stability code ERATO, a quasi-inverse finite hybrid element code has been written. To fit well the plasma surface and the region around the magnetic axis, adequate coordinate transformations are made. A Picard iteration is used to treat the non-linearity of the source term. One Picard step is carried out by solving the weak form of the partial differential equation by an isoparametric finite hybrid element approach (FHE). After each Picard step, the nodal points are readjusted such that they fall on initially prescribed flux surfaces. This enables us to accumulate the nodal points in those regions where good precision is needed for the stability code. While for a conforming finite element scheme a 4-point integration is necessary, a 1-point integration is sufficient in a FHE approach. Coding the FHE is very simple and easily vectorisable. For a given resolution, the precision of global quantities, such as the total flux, is the same for both methods but the FHE approach is faster.

1. INTRODUCTION

Finite difference and finite element methods approximate the exact solution Ψ of a second order partial differential equation in the following way

$$\|\Psi_h - \Psi\| < c \; \mathcal{O}(h^l) \qquad (1)$$

where h and l are measures of the discretization mesh size and the order of the approximation, respectively. The size of the constant c strongly depends on the choice of the coordinate system and on how well the solution is approximated locally. For instance, c becomes big if the boundary is poorly represented.

To obtain a small $\|\Psi_h - \Psi\|$, one can choose between a high order approach (l big), a fine grid (h small) and a formulation leading to a small value of c. However, the computational physicist is also concerned about manpower necessary to achieve those goals and the possibility of vectorizing the computer code. Often, these are reasons why high order approaches are not considered. Also high order approaches can lead to the Gibbs phenomenon (parasit overshoot oscillations) for solutions which rapidely vary locally but are smooth elsewhere (see for instance Ref. [1]). In such situations, mesh accumulation helps to increase precision of the approximate solution. For such cases a finite element method is to prefere to a finite difference method where l is lowered for a nonequidistant mesh. Besides h and l, the constant c in eq. (1) plays an important role for the precision of the approximate solution Ψ_h. It is especially this constant which we try to keep small in our approach. We minimize the error of Ψ_h by:

a) Choosing a coordinate system to represent as closely as possible the boundary and to fit the analytic behaviour of the solution Ψ_h around a particular point in the domain which can be the axis.

b) Readjusting the grid iteratively to fit physically important surfaces.

c) Accumulating the mesh around these surfaces.

d) Choosing nonconforming isoparametric finite hybrid elements instead of conforming isoparametric elements to reduce a 4-point integration scheme to a 1-point integration formula. This reduces computing time of the matrix elements and eases vectorisation.

This proceeding is applied to the fixed boundary Grad-Schlüter-Shafranov equation describing the equilibrium state of a thermonuclear tokamak fusion plasma (see Ref. [2]).

2. PHYSICAL PROBLEM

2.1 Equilibrium equation

In natural units [3] the static ideal MHD equilibrium equations are:

$$\underline{\nabla} p = (\underline{\nabla} \times \underline{B}) \times \underline{B} \qquad (1)$$

$$\underline{\nabla} \cdot \underline{B} = 0 \qquad (2)$$

Let us restrict to axisymmetric geometry for which the toroidal angle ϕ is an ignorable coordinate (Fig. 1). For this geometry, eq. (2) is

satisfied by:

$$\underline{B} = T\underline{\nabla}\phi + \underline{\nabla}\phi \times \underline{\nabla}\Psi. \tag{3}$$

By dotting eq. (1) with $\underline{\nabla}\phi$ and $\underline{B}$ respectively one finds that p and T are constant on constant Ψ-surfaces. Dotting eq. (1) with $\underline{\nabla}\Psi$ gives the Grad-Schlüter-Shafranov equation in the plasma domain Ω

$$r^2\underline{\nabla} \cdot \left(\frac{\underline{\nabla}\Psi}{r^2}\right) = -r^2 \frac{dp}{d\Psi} - T\frac{dT}{d\Psi} = r\mathcal{J}(\Psi,r) \tag{4}$$

where r is the distance from the symmetry axis (see Fig. 1). We restrict ourselves to the fixed boundary problem for which

$$\Psi = 0 \tag{5}$$

at the plasma surface Γ.

To solve eq. (4) one can prescribe two arbitrary functions $p(\Psi)$ and $T(\Psi)$. In general they are nonlinear functions in Ψ. In practice they are chosen such that $\mathcal{J}(\Psi,r) = 0$ at Γ and, as a consequence, the trivial solution $\Psi=0$ satisfies (4) and (5). To prevent this solution we have to normalize our system by demanding, for instance, that the total toroidal current

$$\int_\Omega r\,\underline{\nabla}\phi \cdot (\underline{\nabla}\times\underline{B})\, d^2x = \int_\Omega \mathcal{J}\, d^2x = I \tag{6}$$

be imposed. Here, d^2x is the area element in Ω. Condition (6) can be imposed by scaling the source

$$\mathcal{J} = \lambda \mathcal{J}^* \tag{7}$$

and solving for λ.

2.2 Variational form

Introducing U to be the set of all functions $u \in L^2(\Omega)$[1], $|\underline{\nabla} u| \in L^2(\Omega)$, $u = 0$ at Γ and $u < 0$ in Ω, problem eqs. (4-7) can be written in its weak form (see Ref. [4]):

"Find a real number λ and $\Psi \in U$ such that

$$\int_\Omega \frac{1}{r} \underline{\nabla}\Psi \cdot \underline{\nabla}\eta \, d^2x + \lambda \int_\Omega \mathcal{J}^* d^2x = 0 \qquad (8)$$

for all $\eta \in U$ and that for a given I

$$\lambda \int_\Omega \mathcal{J}^* d^2x = I."$$

2.3 Coordinates to fit Γ and axis

To fit the plasma surface precisely and to guarantee regularity at the magnetic axis, a new coordinate system $(æ,\theta)$ is introduced. It is related to the cylindrical coordinates (r,z) through

$$\begin{aligned} r &= R_0 + \sqrt{æ}\,\rho_\Gamma(\theta)\cos\theta \\ z &= \sqrt{æ}\,\rho_\Gamma(\theta)\sin\theta \end{aligned} \qquad (9)$$

The center of the coordinate system is given by $æ=0$, corresponding to the point $(R_0,0)$ in the (r,z) coordinate system. The plasma surface Γ is given by $æ=1$. The given function $\rho_\Gamma(\theta)$ describes the form of Γ.

2.4 Readjustment and accumulation of the mesh

To guarantee regularity of the solution at the magnetical axis

---

[1] $L^2(\Omega)$ means: square integrable functions in Ω.

and to fit the physically relevent Ψ= constant surfaces, we iteratively readjust the grid. At the end of each Picard step the values of R_0 and æ are recalculated such that the point $r=R_0$, $z=0$ fall on the minimum of Ψ in Ω and that the grid points ($æ_{ij},\theta_j$, $j=1,N_\theta$) fall on prescribed Ψ_i surfaces. This makes it possible to accumulate the grid around singular Ψ surfaces, a proceeding necessary to deliver a precise enough solution to the linear ideal MHD stability code ERATO. We call this a quasi-inverse approach.

3. FORMULATION OF THE APPROXIMATE PROBLEM

3.1 Picard iteration

The nonlinear problem (8) is solved iteratively by a Picard method. Let Ψ^k and λ^k be the approximate solution after k iteration steps. Then Ψ^{k+1} and λ^{k+1} are determined by:
"Find real number λ^{k+1} and $\Psi^{k+1} \in U$ such that[2])

$$\int_\Omega \frac{1}{r} \underline{\nabla}\Psi^{k+1} \cdot \underline{\nabla}\eta d^2x + \lambda^k \int_\Omega \mathcal{J}^{*k} \eta d^2x = 0 \qquad (10)$$

for all $\eta \in U$ and that for a given value of I

$$\lambda^{k+1} \int_\Omega \mathcal{J}^{*k+1} d^2x = I."$$

As an initial guess Ψ^0 one often takes a previously calculated solution in the same domain Ω and for slightly different parameters in the source function. In most of the practical cases, Picard method

---

[2]) $\mathcal{J}^{*k}$ means: evaluate $\mathcal{J}^*$ using Ψ^k.

converges. In the few cases that it does not converge, a continuation method can be used (see Ref. [5]).

3.2 Conforming approximation

Let us subdivide the domain Ω in N_r x N_z or N_{ϖ} x N_θ mesh cells and U_h be a finite dimensional subspace of U. A Ritz-Galerkin method for approximating the eigenelements $(\Psi^{k+1},\lambda^{k+1})$ of formulation (10) consists to

"Find real numbers $\lambda_h{}^{k+1}$ and functions $\Psi_h{}^{k+1} \varepsilon U_h$ such that

$$\int_\Omega \frac{1}{r} \underline{\nabla}\Psi_h^{k+1} \cdot \underline{\nabla}\eta_h \, d^2x + \lambda_h^k \int_\Omega \mathscr{S}_h^{*k} \eta_h \, d^2 x = 0 \qquad (11)$$

for all $\eta_h \varepsilon U_h$ and that for a given I

$$\lambda_h^{k+1} \int_\Omega \mathscr{S}_h^{*k+1} \, d^2x = I."$$

In (r,z) coordinates U_h is the set of all functions $u_h \varepsilon L^2(\Omega)$, $\partial u_h/\partial r \varepsilon L^2(\Omega)$, $\partial u_h/\partial z \varepsilon L^2(\Omega)$, $u_h = 0$ at Γ and $u_h < 0$ in Ω. Formulation (11) then writes

"Find real numbers $\lambda_h{}^{k+1}$ and functions $\Psi_h{}^{k+1} \varepsilon U_h$ such that

$$\int_\Omega \frac{1}{r} \left(\frac{\partial\Psi_h^{k+1}}{\partial r}\frac{\partial\eta_h}{\partial r} + \frac{\partial\Psi_h^{k+1}}{\partial z}\frac{\partial\eta_h}{\partial z}\right) drdz + \lambda_h^k \int_\Omega \mathscr{S}_h^{*k} \eta_h \, drdz = 0 \qquad (12)$$

for all $\eta_h \varepsilon U_h$ and that for a given I

$$\lambda_h^{k+1} \int_\Omega \mathscr{S}_h^{*k+1} \, drdz = I."$$

In (æ,θ) coordinates $\Omega = \{0<æ<1,\ 0<\theta<2\pi\}$, $\Gamma = \{æ=1,\ 0<\theta<2\pi\}$ and U_h is the set of all functions $u_h \in L^2(\Omega)$, $\partial u_h/\partial æ \in L^2(\Omega)$, $\partial u_h/\partial\theta \in L^2(\Omega)$, $u_h(æ=1,\theta) = 0$, $u_h(æ,\theta) = u_h(æ,\theta+2L\pi)$, L integer, and $u_h < 0$ in Ω. Formulation (11) then writes:

"Find real number λ_h^{k+1} and functions $\Psi_h^{k+1} \in U_h$ such that

$$\int_0^1 dæ \int_0^{2\pi} \frac{æ}{r}\left[\frac{\partial\Psi_h^{k+1}}{\partial æ}\frac{\partial\eta_h}{\partial æ} + \left(\frac{1}{2æ}\frac{\partial\Psi_h^{k+1}}{\partial\theta} - \frac{\frac{d\rho_\Gamma}{d\theta}}{\rho_\Gamma}\frac{\partial\Psi_h^{k+1}}{\partial æ}\right)\left(\frac{1}{2æ}\frac{\partial\eta_h}{\partial\theta} - \frac{\frac{d\rho_\Gamma}{d\theta}}{\rho_\Gamma}\frac{\partial\eta_h}{\partial æ}\right)\right]d\theta$$

$$= \frac{1}{4}\lambda_h^k \int_0^1 dæ \int_0^{2\pi} \rho_\Gamma^2\,\eta_h\,\mathcal{J}_h^{*k}\,d\theta \qquad (13)$$

for all $\eta_h \in U_h$ and for a given I

$$\frac{1}{2}\lambda_h^{k+1} \int_0^1 dæ \int_0^{2\pi} \rho_\Gamma^2\,\mathcal{J}_h^{*k+1}\,d\theta = I."$$

3.3 Non-conforming approximation

In addition to U_h, let us introduce 3 finite dimensional spaces:

U_1 is the set of all functions $u_1 \in L^2(\Omega)$, $u_1(æ=1,\theta) = 0$, $u_1(æ,\theta) = u_1(æ,\theta+2L\pi)$, L integer, and $u_1 < 0$ in Ω,

U_2 is the set of all functions $u_2 \in L^2(\Omega)$, $\partial u_2/\partial æ \in L^2(\Omega)$, $u_2(æ=1,\theta) = 0$, $u_2(æ,\theta) = u_2(æ,\theta+2L\pi)$, L integer, and $u_2 < 0$ in Ω and

U_3 is the set of all functions $u_3 \in L^2(\Omega)$, $\partial u_3/\partial\theta \in L^2(\Omega)$, $u_3(æ=1,\theta) = 0$, $u_3(æ,\theta) = u_3(æ,\theta+2L\pi)$, L integer and $u_3 < 0$ in Ω.

Formulation (13) can then be rewritten in a more complicated way: "Find real numbers λ_h^{k+1} and functions $\Psi_h^{k+1} \in U_h$, $\Psi_1 \in U_1$,

$\Psi_2 \in U_2$ and $\Psi_3 \in U_3$ such that[3)]

$$\int_0^1 d\text{æ} \int_0^{2\pi} \frac{\text{æ}}{r} \left[\frac{\partial \Psi_2}{\partial \text{æ}} \frac{\partial \eta_2}{\partial \text{æ}} + \left(\frac{1}{2\text{æ}} \frac{\partial \Psi_3}{\partial \theta} - \frac{\frac{d\rho_\Gamma}{d\theta}}{\rho_\Gamma} \frac{\partial \Psi_2}{\partial \text{æ}} \right) \left(\frac{1}{2\text{æ}} \frac{\partial \eta_3}{\partial \theta} - \frac{\frac{d\rho_\Gamma}{d\theta}}{\rho_\Gamma} \frac{\partial \eta_2}{\partial \text{æ}} \right) \right] d\theta$$

$$= \frac{1}{4} \lambda_h^k \int_0^1 d\text{æ} \int_0^{2\pi} \rho_\Gamma^2 \, \eta_1 \, \mathcal{J}_1^{*k} \, d\theta \qquad (14)$$

for all $\eta_1 \in U_1$, $\eta_2 \in U_2$, $\eta_3 \in U_3$, that

$$\int_0^1 d\text{æ} \int_0^{2\pi} (\Psi_h^{k+1} - \Psi_i) \, \xi_i \, d\theta = 0 \quad , \quad i = 1,2,3 \qquad (15)$$

for all $\xi_i \in L^2(\Omega)$, $i = 1,2,3$

and that for a given I

$$\frac{1}{2} \lambda_h^{k+1} \int_0^1 d\text{æ} \int_0^{2\pi} \rho_\Gamma^2 \, \mathcal{J}_1^{*k+1} \, d\theta = I." \qquad (16)$$

Note that formulations (13) and (14-16) are identical since the integral conditions (15) imply that

$$\Psi_i = \Psi_h^{k+1} \qquad i = 1,2,3 \qquad (17)$$

However, they differ if the functions ξ_i, $i = 1,2,3$ are chosen in a finite dimensional function space.

4. LOWEST ORDER FINITE ELEMENTS

4.1 Choice of finite elements

In a first step we subdivide the domain $\Omega = \{0<\text{æ}<1, \ 0<\theta<2\pi\}$ into $N_{\text{æ}} \times N_\theta$ rectangular mesh cells. As functions η_h, η_1, η_2, η_3,

---

[3)] $\mathcal{J}_1^{*k}$ means: evaluate $\mathcal{J}_1^{*k}$ using Ψ_1^k.

ξ_1, ξ_2 and ξ_3 we choose bilinear finite elements defined by (i=1,..., $N_{æ}$; j=1,..., N_θ).

$$\begin{aligned} \eta_h &= e_i(æ) \cdot e_j(\theta) \\ \eta_1 &= c_{i-1/2}(æ) \cdot c_{j-1/2}(\theta) \\ \eta_2 &= e_i(æ) \cdot c_{j-1/2}(\theta) \\ \eta_3 &= c_{i-1/2}(æ) \cdot e_j(\theta) \\ \xi_1 = \xi_2 = \xi_3 &= c_{i-1/2}(æ) \cdot c_{j-1/2}(\theta) \end{aligned} \tag{18}$$

The finite elements $c_k(x)$ and $e_k(x)$ are

$$c_k(x) = \begin{cases} 0 & x_0 < x < x_{k-1} \\ 1 & x_{k-1} < x < x_k \\ 0 & x_k < x < x_N \end{cases} \tag{19}$$

$$e_k(x) = \begin{cases} 0 & , x_0 < x < x_{k-1} \\ \dfrac{x-x_{k-1}}{x_k-x_{k-1}} & , x_{k-1} < x \leq x_k \\ \dfrac{x_{k+1}-x}{x_{k+1}-x_k} & , x_k \leq x < x_{k+1} \\ 0 & , x_{k+1} < x < x_N \end{cases} \tag{20}$$

The unknowns Ψ_h^{k+1}, Ψ_1, Ψ_2 and Ψ_3 are expanded in terms of these finite elements:

$$\begin{aligned} \Psi_h^{k+1}(æ,\theta) &= \sum_{i=0}^{N_{æ}-1} \sum_{j=0}^{N_\theta} \Psi_{ij}\, e_i(æ)\, e_j(\theta) \\ \Psi_1(æ,\theta) &= \sum_{i=1}^{N_{æ}} \sum_{j=1}^{N_\theta} \Psi_{i-1/2j-1/2}\, c_{i-1/2}(æ)\, c_{j-1/2}(\theta) \end{aligned} \tag{21}$$

$$\Psi_2(æ,\theta) = \sum_{i=0}^{N_{æ}-1} \sum_{j=1}^{N_\theta} \Psi_{ij-1/2}\, e_i(æ)\, c_{j-1/2}(\theta)$$

$$\Psi_3(æ,\theta) = \sum_{i=1}^{N_{æ}} \sum_{j=0}^{N_\theta} \Psi_{i-1/2j}\, c_{i-1/2}(æ)\, e_j(\theta)$$

4.2 Conforming isoparametric finite elements

By choosing bilinear finite elements, eqs. (21), to represent Ψ_h^{k+1}, the integrals in the formulation (13) have to be performed by a 4 point Gauss formula.

Let us now discretize the domain Ω into $N_{æ} \times N_\theta$ quadrangular (non-rectangular) mesh cells. In this case we have to perform local variable transformations $(æ,\theta) \to (\xi,\chi)$ of the form

$$\begin{aligned} æ(\xi,\chi) &= \alpha_1 + \alpha_2\xi + \alpha_3\chi + \alpha_4\xi\chi \\ \theta(\xi,\chi) &= \beta_1 + \beta_2\xi + \beta_3\chi + \beta_4\xi\chi \end{aligned} \qquad (22)$$

The eight parameters α_1 to α_4 and β_1 to β_4 are determined by the coordinates $æ_1$ to $æ_4$ and θ_1 to θ_4 (see Fig. 2)

$$\begin{aligned} \alpha_1 &= æ_1 & \beta_1 &= \theta_1 \\ \alpha_2 &= æ_2 - æ_1 & \beta_2 &= \theta_2 - \theta_1 \\ \alpha_3 &= æ_4 - æ_1 & \beta_3 &= \theta_4 - \theta_1 \\ \alpha_4 &= æ_1 + æ_3 - æ_2 - æ_4 & \beta_4 &= \theta_1 + \theta_3 - \theta_2 - \theta_4 \end{aligned} \qquad (23)$$

In order to prevent problems concerning integration and uniqueness of the transformation (23), we demand that all angles of the quadrangles be smaller than π.

By transforming from $(æ,\theta)$ to (ξ,χ) the surface element becomes

$$dæ\, d\theta = J d\xi d\chi, \tag{24}$$

where

$$J = \frac{1}{\frac{\partial\xi}{\partial æ}\frac{\partial\chi}{\partial\theta} - \frac{\partial\xi}{\partial\theta}\frac{\partial\chi}{\partial æ}} = (\alpha_2 + \alpha_4\chi)(\beta_3 + \beta_4\xi) - (\beta_2 + \beta_4\chi)(\alpha_3 + \alpha_4\xi) \tag{25}$$

is the Jacobian. In these new (ξ,χ) coordinates the derivatives of any quantity A become

$$\begin{aligned} J\frac{\partial A}{\partial æ} &= (\beta_3 + \beta_4\xi)\frac{\partial A}{\partial\xi} - (\beta_2 + \beta_4\chi)\frac{\partial A}{\partial\chi} \\ J\frac{\partial A}{\partial\theta} &= -(\alpha_3 + \alpha_4\xi)\frac{\partial A}{\partial\xi} + (\alpha_2 + \alpha_4\chi)\frac{\partial A}{\partial\chi} \quad . \end{aligned} \tag{26}$$

One has to note that these formulae are still valid when the quadrangle degenerates into a triangle as can happen at the origin of a cylindrical coordinate system.

The finite elements have now to be understood in such a way that $c_{k-1/2}(x)$ be piecewise constant in ξ or χ and that $e_k(x)$ be linear in ξ or in χ. The precise functional dependences of the elements in the $(æ,\theta)$ plane can be found through the transformation (22).

In practice, one knows the coordinates æ and θ of the 4 edge points of a cell. These define the transformation eqs. (23) and, consequently, the Jacobian through eq. (25). The 4 point Gauss integration is performed in the (ξ,χ) plane. To know all the quantities a back-transformation is necessary to know the positions of the Gauss points in the $(æ,\theta)$ plane.

4.3 Non conforming isoparametric finite hybrid elements

Let us first consider the case of a rectangular $(æ,\theta)$ mesh. Choosing for η_h, η_1, η_2, η_3, ξ_1, ξ_2 and ξ_3 the elements of eqs. (18) and for Ψ_h^{k+1}, Ψ_1, Ψ_2 and Ψ_3 the expansions eqs. (21), the integral conditions, eqs. (15) in the formulation eqs. (14-16) correspond to

$$\begin{aligned} \Psi_{i-1/2j-1/2} &= \frac{1}{4}\left(\Psi_{i-1j-1} + \Psi_{ij-1} + \Psi_{i-1j} + \Psi_{ij}\right) \\ \Psi_{ij-1/2} &= \frac{1}{2}\left(\Psi_{ij-1} + \Psi_{ij}\right) \\ \Psi_{i-1/2j} &= \frac{1}{2}\left(\Psi_{i-1j} + \Psi_{ij}\right) \end{aligned} \tag{27}$$

As a consequence, the derivatives of Ψ_2 with respect to æ and Ψ_3 with respect to θ become centred finite differences

$$\begin{aligned} \frac{\partial \Psi_2}{\partial æ}\left(æ_{i-\frac{1}{2}j-\frac{1}{2}}, \vartheta_{i-\frac{1}{2}j-\frac{1}{2}}\right) &= \frac{\Psi_{ij-1} + \Psi_{ij} - \Psi_{i-1j-1} - \Psi_{i-1j}}{2\left(æ_{ij} - æ_{i-1j-1}\right)} \\ \frac{\partial \Psi_3}{\partial \vartheta}\left(æ_{i-\frac{1}{2}j-\frac{1}{2}}, \vartheta_{i-\frac{1}{2}j-\frac{1}{2}}\right) &= \frac{\Psi_{ij} + \Psi_{i-1j} - \Psi_{ij-1} - \Psi_{i-1j-1}}{2\left(\vartheta_{ij} - \vartheta_{i-1j-1}\right)} \end{aligned} \tag{28}$$

It is this fact which gave us the idea to call this non-conforming approach "finite hybrid element method".

All the quantities in eqs. (14) and (16) including η and Ψ are now piecewise constant in each mesh cell. If, in each mesh cell, we approximate all the coefficients, i.e. æ, ρ_Γ and $d\rho_\Gamma/d\theta$, by their values at the centre of the cell, the integrals in eqs. (14) and (16)

simply become

$$\int_0^1 d\chi \int_0^{2\pi} A(\chi,\vartheta)\,d\vartheta = \sum_{i=1}^{N_\chi}\sum_{j=1}^{N_\vartheta} A\left(\chi_{i-\frac{1}{2}\,j-\frac{1}{2}},\vartheta_{i-\frac{1}{2}\,j-\frac{1}{2}}\right)\left(\chi_{ij}-\chi_{i-1\,j}\right)\left(\vartheta_{ij}-\vartheta_{i\,j-1}\right) \tag{29}$$

Let us consider now the case of a quadrangular, i.e. non-rectangular mesh. Again we perform a local variable transformation as given by eqs. (22). Choosing again all the quantities to be piecewise constant in a (ξ,χ) cell, a one point integration formula is again sufficient and can directly be written in the $(\text{æ},\theta)$ plane:

$$\int_0^1 d\chi \int_0^{2\pi} A(\chi,\vartheta)\,d\vartheta = \sum_{i=1}^{N_\chi}\sum_{j=1}^{N_\vartheta} A\left(\bar{\chi}_{i-\frac{1}{2}\,j-\frac{1}{2}},\bar{\vartheta}_{i-\frac{1}{2}\,j-\frac{1}{2}}\right) J_{i-\frac{1}{2}\,j-\frac{1}{2}}$$

where

$$\bar{\chi}_{i-\frac{1}{2}\,j-\frac{1}{2}} = \frac{1}{4}\left(\chi_{i-1\,j-1}+\chi_{i\,j-1}+\chi_{i-1\,j}+\chi_{ij}\right)$$

$$\bar{\vartheta}_{i-\frac{1}{2}\,j-\frac{1}{2}} = \frac{1}{4}\left(\vartheta_{i-1\,j-1}+\vartheta_{i\,j-1}+\vartheta_{i-1\,j}+\vartheta_{ij}\right) \tag{30}$$

$$J_{i-\frac{1}{2}\,j-\frac{1}{2}} = \frac{1}{2}\left[\left(\vartheta_{i-1\,j}-\vartheta_{i\,j-1}\right)\left(\chi_{ij}-\chi_{i-1\,j-1}\right)+\left(\vartheta_{ij}-\vartheta_{i-1\,j-1}\right)\left(\chi_{i\,j-1}-\chi_{i-1\,j}\right)\right]$$

The quantities in eq. (14) including Ψ become

$$\Psi_1\left(\bar{\chi}_{i-\frac{1}{2}\,j-\frac{1}{2}},\bar{\vartheta}_{i-\frac{1}{2}\,j-\frac{1}{2}}\right) = \frac{1}{2}\left(\Psi_{i-1\,j-1}+\Psi_{i\,j-1}+\Psi_{i-1\,j}+\Psi_{ij}\right)$$

$$\frac{\partial\Psi_2}{\partial\chi}\left(\bar{\chi}_{i-\frac{1}{2}\,j-\frac{1}{2}},\bar{\vartheta}_{i-\frac{1}{2}\,j-\frac{1}{2}}\right) = \frac{1}{2J_{i-\frac{1}{2}\,j-\frac{1}{2}}}\left[\left(\vartheta_{i-1\,j}-\vartheta_{i\,j-1}\right)\left(\Psi_{ij}-\Psi_{i-1\,j-1}\right)\right. \tag{31}$$

$$\left.+\left(\vartheta_{ij}-\vartheta_{i-1\,j-1}\right)\left(\Psi_{i\,j-1}-\Psi_{i-1\,j}\right)\right]$$

$$\frac{\partial \psi_3}{\partial \vartheta}\left(\bar{\chi}_{i-\frac{1}{2}j-\frac{1}{2}}, \bar{\vartheta}_{i-\frac{1}{2}j-\frac{1}{2}}\right) = \frac{1}{2\,J_{i-\frac{1}{2}j-\frac{1}{2}}}\Big[\left(\chi_{ij-1}-\chi_{i-1j}\right)\left(\psi_{ij}-\psi_{i-1j-1}\right) + \left(\chi_{i-1j-1}-\chi_{ij}\right)\left(\psi_{ij-1}-\psi_{i-1j}\right)\Big]$$

For the test functions η one has to take the values at the centre of the (ξ,χ) cells and transform them back to the $(æ,\theta)$ plane. The test functions attributed to the 4 nodal values Ψ_{i-1j-1}, Ψ_{ij-1}, Ψ_{i-1}, Ψ_{ij} in the mesh cell are

$$\eta_1 = \left(\frac{1}{4}, \frac{1}{4}, \frac{1}{4}, \frac{1}{4}\right)$$

$$\frac{\partial \eta_2}{\partial \chi} = \left(-\frac{\vartheta_{i-1j}-\vartheta_{ij-1}}{2\,J_{i-\frac{1}{2}j-\frac{1}{2}}}, \frac{\vartheta_{ij}-\vartheta_{i-1j-1}}{2\,J_{i-\frac{1}{2}j-\frac{1}{2}}}, \frac{\vartheta_{i-1j}-\vartheta_{ij-1}}{2\,J_{i-\frac{1}{2}j-\frac{1}{2}}}, -\frac{\vartheta_{ij}-\vartheta_{i-1j-1}}{2\,J_{i-\frac{1}{2}j-\frac{1}{2}}}\right) \quad (32)$$

$$\frac{\partial \eta_3}{\partial \vartheta} = \left(\frac{\chi_{i-1j}-\chi_{ij-1}}{2\,J_{i-\frac{1}{2}j-\frac{1}{2}}}, -\frac{\chi_{ij}-\chi_{i-1j-1}}{2\,J_{i-\frac{1}{2}j-\frac{1}{2}}}, -\frac{\chi_{i-1j}-\chi_{ij-1}}{2\,J_{i-\frac{1}{2}j-\frac{1}{2}}}, \frac{\chi_{ij}-\chi_{i-1j-1}}{2\,J_{i-\frac{1}{2}j-\frac{1}{2}}}\right)$$

A practicle application of the finite hybrid elements with the corresponding computer code is presented in Ref. [1] for the case of the linear ideal MHD stability code ERATO for a toroidal geometry.

5. RESULTS

5.1 Solovev equilibrium

Let us first compare the conforming and the nonconforming hybrid element approaches using the analytic Solovev equilibrium solution given by

$$\frac{dp}{d\Psi} = -2\Psi_S\,(1+E^2)/a^2E^2$$

$$\frac{dT^2}{d\Psi} = 0 \quad (33)$$

and the surface parametrization $\rho_\Gamma(\theta)$ by

$$a^2 = E^{-2}(1+\rho_\Gamma(\theta)\cos\theta)^2\ \rho^2{}_\Gamma(\theta)\ \sin^2\theta \qquad (34)$$

$$+\ 0.25\ (2+\rho_\Gamma(\theta)\cos\theta)^2\ \rho^2{}_\Gamma(\theta)\ \cos^2\theta$$

Here, a, E and Ψ_S denote the inverse aspect ratio, the elongation and the total flux. The position of the magnetic axis is at $r=R_0=1$. Note that $\rho_\Gamma(0) = \sqrt{1+2a} - 1$ and $\rho_\Gamma(\pi) = 1-\sqrt{1-2a}$.

In Fig. 3 we show convergence studies of the approximated solutions corresponding to the set of parameters a=0.4, E=1 and $dp/d\Psi=-2$. We see that both methods, the conforming and the hybrid finite elements, converge quadratically toward the exact values of $\Psi_S=0.08$ and $R_0=1$, the slope of the convergence curve for the hybrid elements being smaller. This means that the value of c in eq. (1) is smaller for the nonconforming approach than for the conforming one.

For the case with a=0.4, E=2 and $dp/d\Psi=-2.5$ we see in Fig. 4 that the conforming approach has similar convergence behaviour as the hybrid one. In Fig. 5 we show the convergence behaviour of the quantity Ψ_S fixing either $N_{\alpha}=20$ or $N_\theta=20$. The error for $N_{\alpha}=20$ is much smaller than that for $N_\theta=20$. We find that N_θ of the order of $\sim 3N_{\alpha}$ is necessary for a balanced convergence study.

Fixing the elongation at E=2 and $dp/d\Psi=2.5$ and increasing the aspect ratio such that a=0.25 the convergence properties of the conforming approach are superior to those of the hybrid approach as we can see in Fig. 6. This is due to the superior integration formula (4

point Gauss integration formula) used for the conforming elements which helps to better approach the plasma surface term including $(d\rho_\Gamma/d\theta)/\rho$ in eq. (13). Comparing these results with those presented in Ref. [4] using (r,z) coordinates, eq. (12), one realizes that using (æ,θ) coordinates 3 to 10 times less intervals have to be taken in both directions to obtain the same precision.

5.2 JET equilibrium

As a practicle application we calculate the equilibrium solution for a JET (Joint European Torus) geometry. The parameters of the JET tokamak are: R_0=2.96 m, a=0.423, T=10.4 Tm, E=1.68 and I=4.8x10^6 A. For the two free functions of the source term we choose

$$p(\Psi/\Psi_s) = 38.1\,(\Psi/\Psi_s)^2 - 5.2\,(\Psi/\Psi_s)^3 \quad N/cm^2$$
$$T^2(\Psi/\Psi_s) = 110 - 2.85\,(\Psi/\Psi_s)^2 \quad T^2m^2 \qquad (35)$$

which corresponds to a case with β=2.5% close to the Troyon stability limit [1,6]. The plasma surface Γ is D shaped and given by

$$r_\Gamma = 2.96\ (1+a\cos(\theta+0.3\ \sin\theta))\ m$$
$$z_\Gamma = 2.96 \cdot E\ a\ \sin\theta\ m \qquad (36)$$

The quasi-inverse solution æ(Ψ,θ) found by adjusting æ such that the grid points fall on Ψ=constant surfaces is represented in the (r,z) plane in Fig. 1. The convergence properties for the conforming and finite hybrid element approaches are shown in Fig. 7. As for the Solovev case the finite hybrid elements have at least as good convergence properties as the conforming elements.

6. CONCLUSIONS

We have compared two finite element approaches, the conforming and a non-conforming one by applying them to the Grad-Schlüter-Shafranov equation. It is found that the non-conforming finite hybrid element approach mostly shows a better convergence behaviour for the global quantities such as total flux or position of the magnetic axis. This hybrid approach is easier to implement and only needs a one point integration formula for the calculation of the matrix elements. This property eases full vectorization of the matrix construction. After their success in the stability problem (Ref. [1]), the hybrid elements have also shown their superiority to the conforming elements in the calculation of ideal fixed boundary MHD equilibria.

REFERENCES

[1] R. Gruber and J. Rappaz, "Finite Element Methods in Linear Ideal Magnetohydrodynamics", Springer Series in Computational Physics (Springer Verlag, 1985)

[2] Proceedings of the 2nd European Workshop on Computational Problems in the Calculation of MHD Equilibria (Wildhaus, 12-14 September 1983) published in Comput. Phys. Commun. 31 (1984) 115-285; Comput. Phys. Reports 1 (1984) 345-494
L.M. Degtyarev and V.V. Drozdov, Comput. Phys. Reports 2 (1985) 341-378

[3] E.S. Weibel, Am. J. Phys. 36 (1968) 1130

[4] S. Semenzato, R. Gruber and H.P. Zehrfeld, Comput. Phys. Reports 1 (1984) 389

[5] J. Blum, J. Le Foll and B. Thorris, Comput. Phys. Commun. 24 (1981) 235

[6] F. Troyon, R. Gruber, H. Saurenmann, S. Semenzato and S. Succi, Plasma Physics 26, 1A (1983) 209-215

FIGURE CAPTIONS

Fig. 1: The axisymmetric geometry for JET. Quasi-inverse solution $æ(\Psi,\theta)$ in the (r,z) plane using finite hybrid element.

Fig. 2: Transformation from a quadrangular cell in the $(æ,\theta)$ plane to a unit square in the (ξ,χ) plane.

Fig. 3: Convergence studies for the total poloidal flux Ψ_S and the position of the magnetic axis R_0 for the conforming and finite hybrid element approaches. Solovev equilibrium: E=1, a=0.4, $dp/d\Psi=-2$. The analytic values are $\Psi_S=.08$ and $R_0=1$.

Fig. 4: Convergence studies for Ψ_S and R_0 for the conforming and finite hybrid element approaches. Solovev equilibrium: E=2, A=0.4, $dp/d\Psi=-2.5$. The analytic values are $\Psi_S=.16$ and $R_0=1$.

Fig. 5: Finite hybrid elements: convergence studies in N_θ for fixed $N_{æ}=20$ and in $N_{æ}$ for fixed $N_\theta=20$.

Fig. 6: Convergence studies for Ψ_S for the conforming and finite hybrid element approaches. Solovev equilibrium: E=2, a=0.25, $dp/d\Psi=-2.5$. The analytic value is $\Psi_S=0.0625$.

Fig. 7: JET geometry: convergence studies for Ψ_S and R_0 for conforming and finite hybrid element approaches.

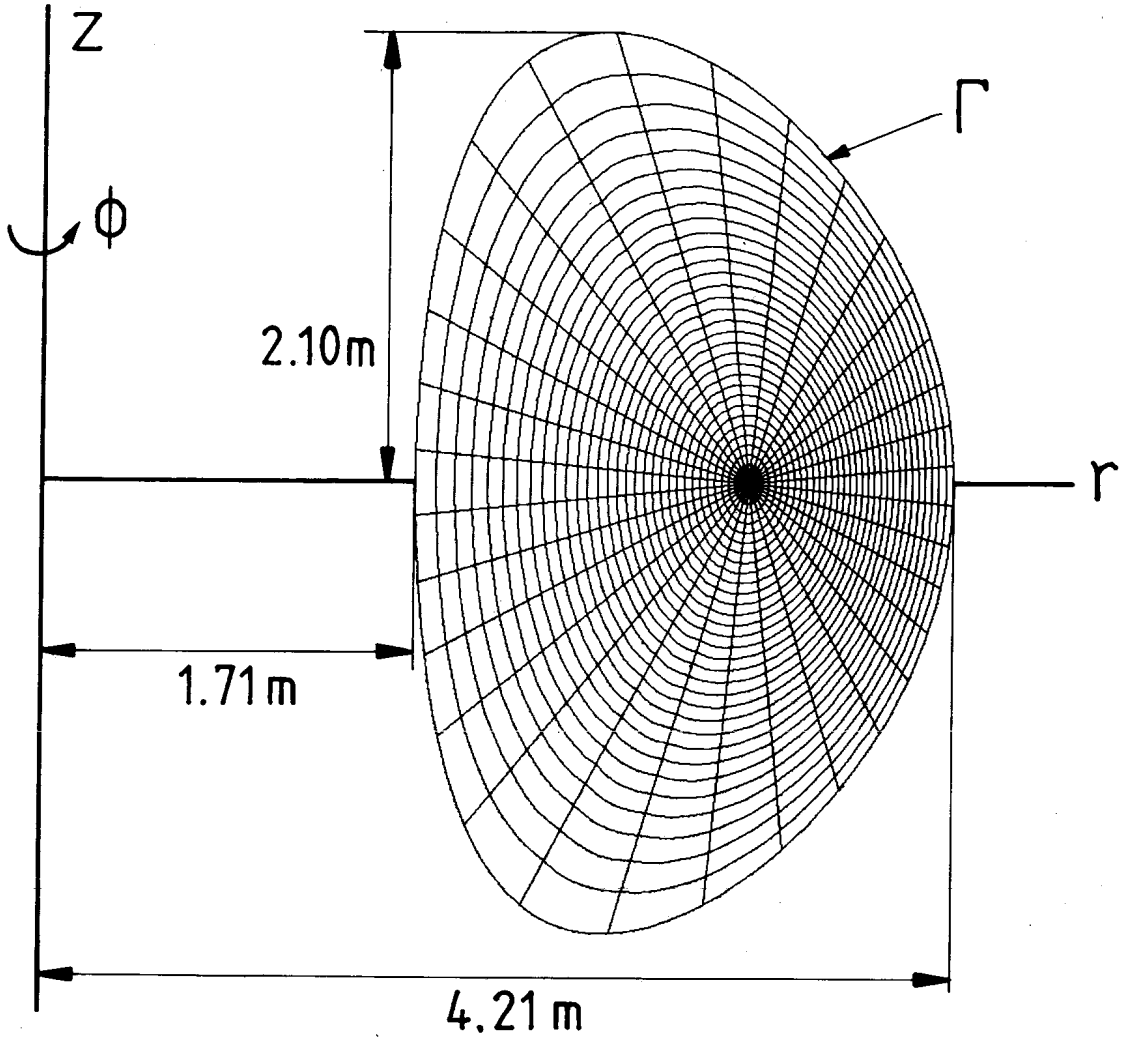
z
ϕ
Γ
2.10m
r
1.71m
4.21m

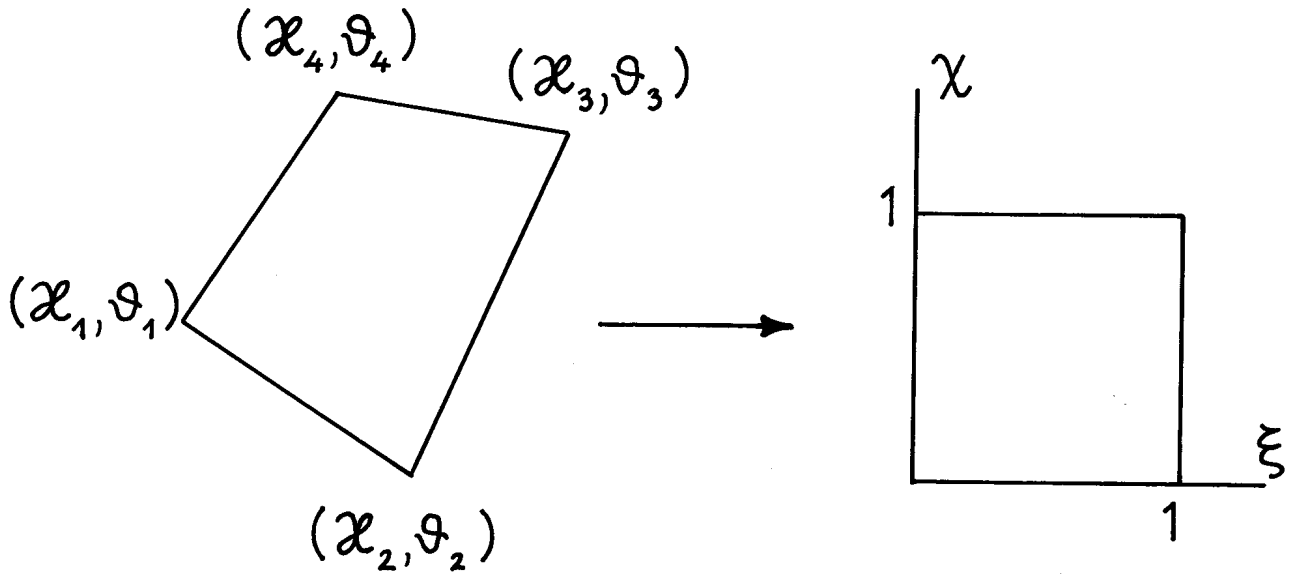
(x_4, ϑ_4)
(x_3, ϑ_3)
(x_1, ϑ_1)
(x_2, ϑ_2)
χ
1
ξ
1

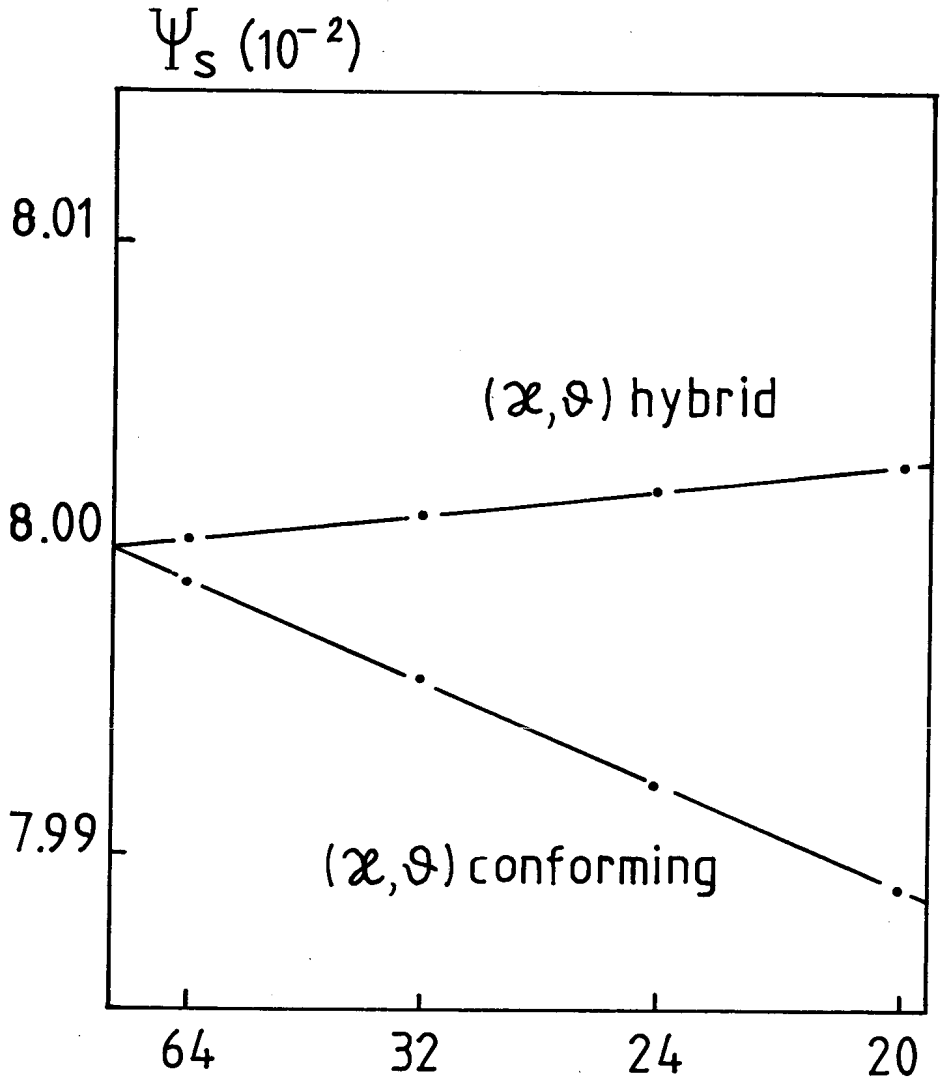
Ψ_s (10^{-2})
8.01
8.00
7.99
$(\mathcal{X},\vartheta)$ hybrid
$(\mathcal{X},\vartheta)$ conforming
64
32
24
20

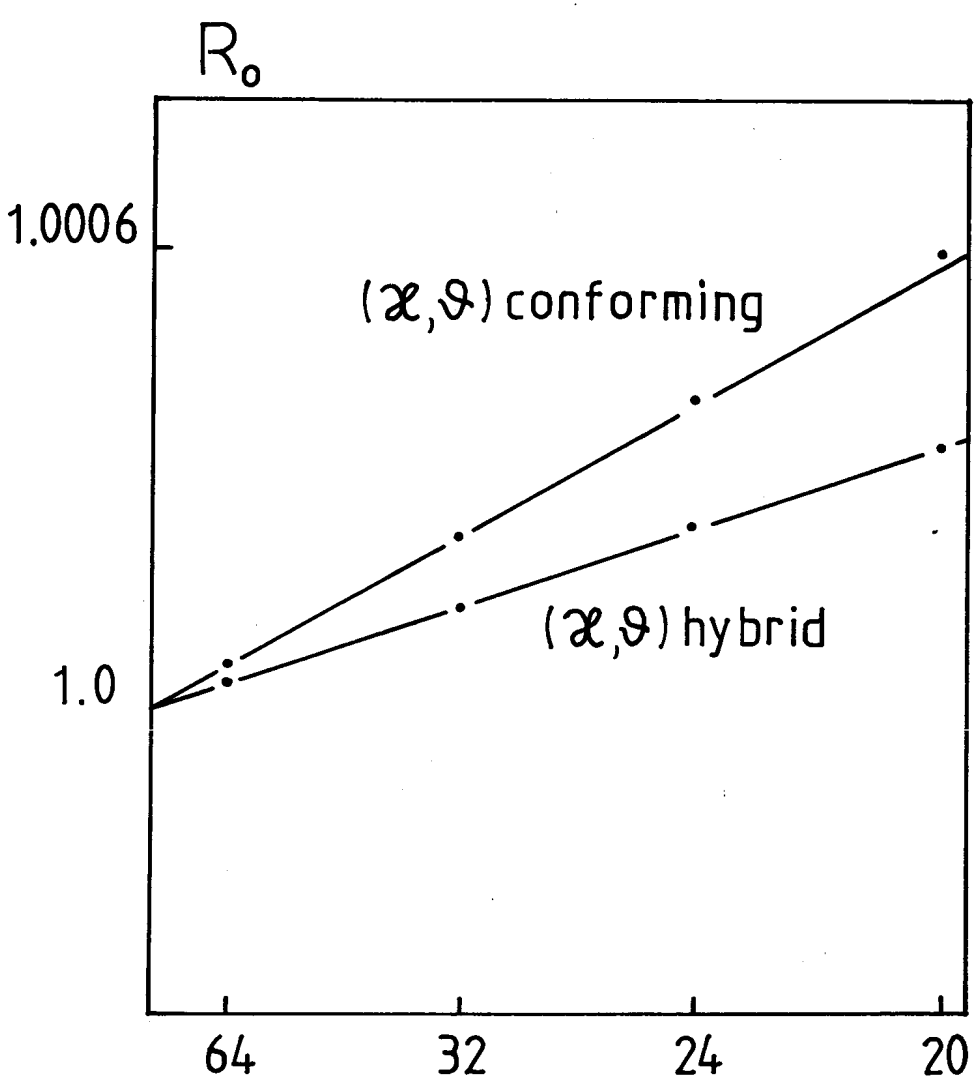
R_o
1.0006
1.0
$(\mathcal{X},\vartheta)$ conforming
$(\mathcal{X},\vartheta)$ hybrid
64
32
24
20

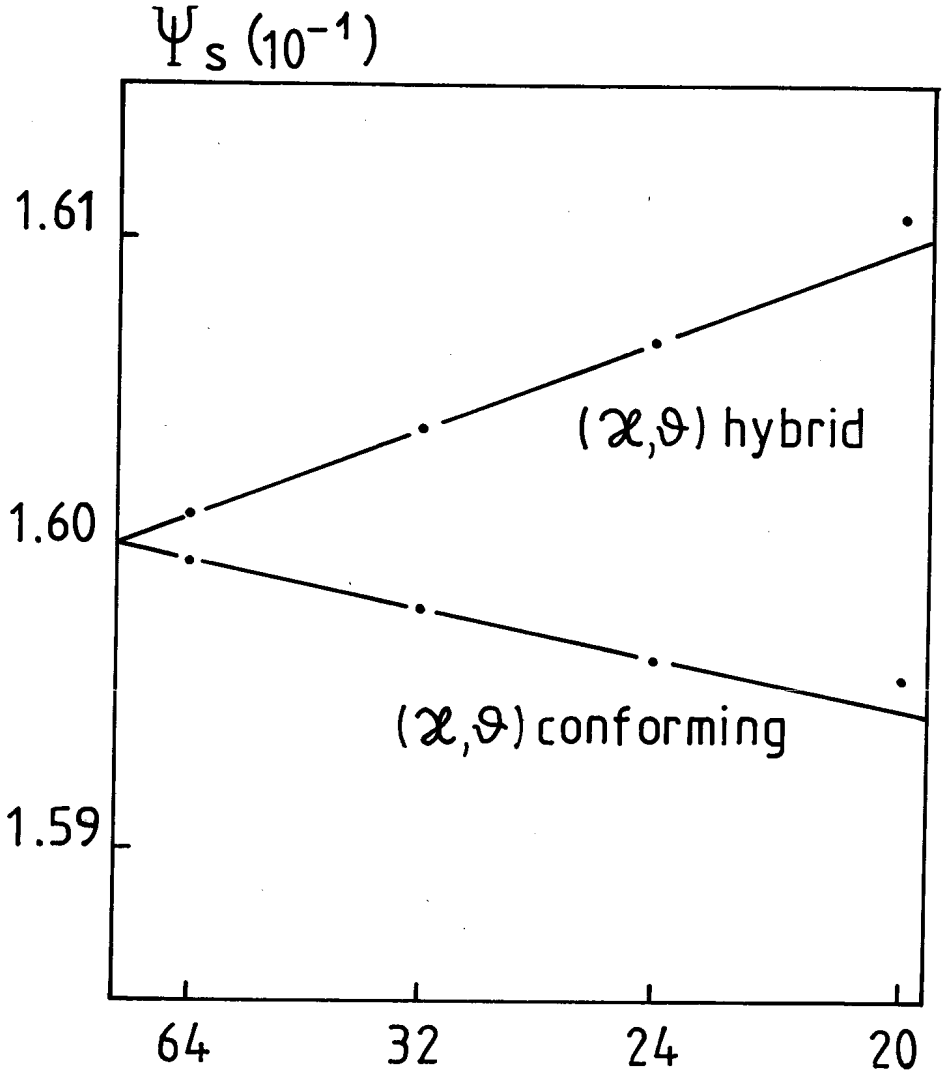
Ψ_s (10^{-1})
1.61
1.60
1.59
(ϰ,ϑ) hybrid
(ϰ,ϑ) conforming
64
32
24
20

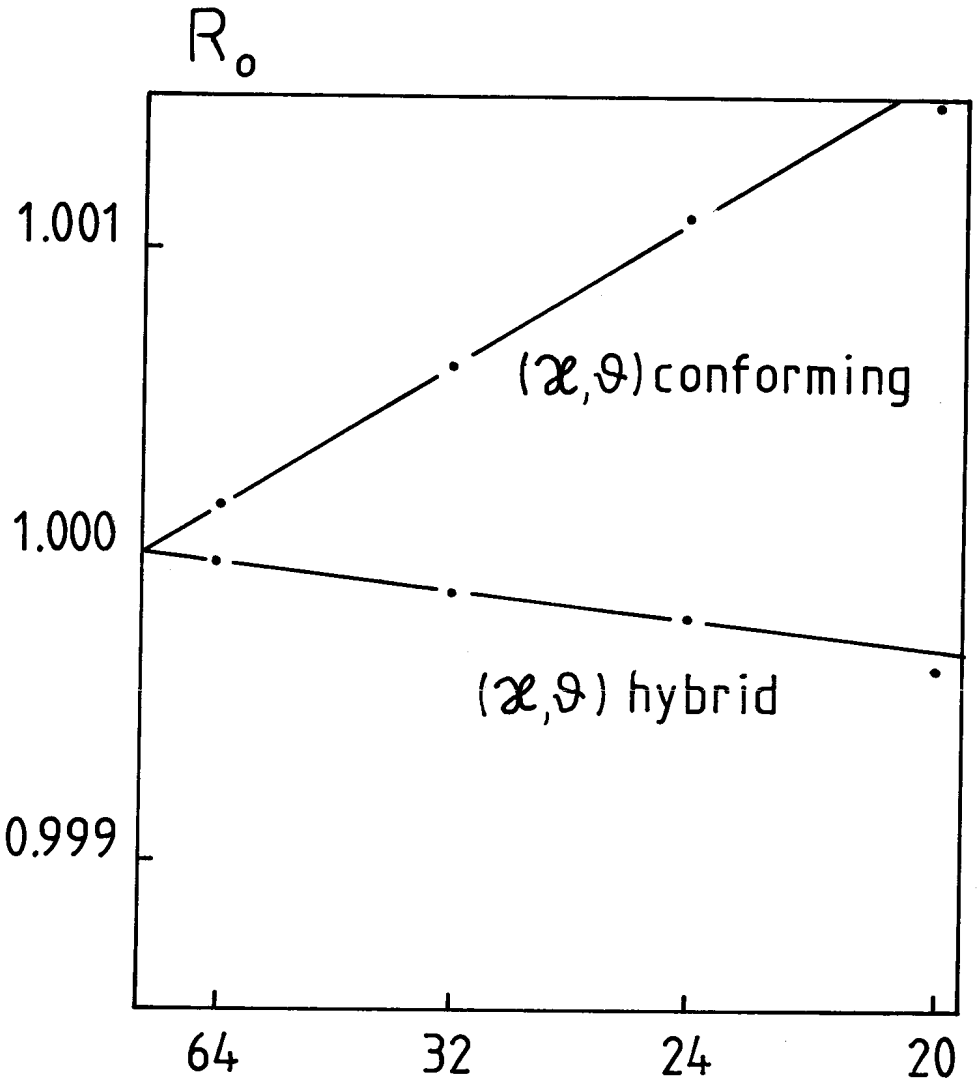
R_o
1.001
1.000
0.999
(ϰ,ϑ) conforming
(ϰ,ϑ) hybrid
64
32
24
20

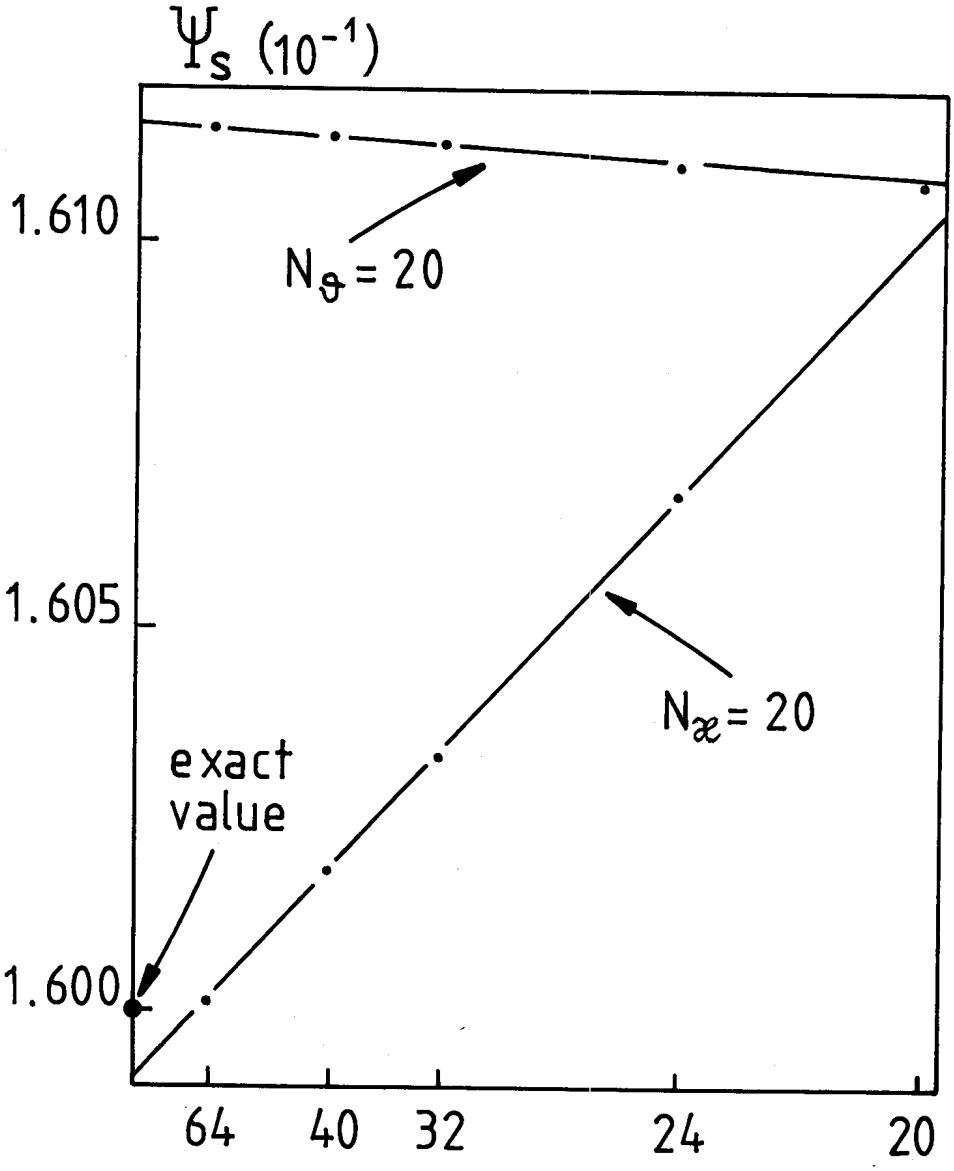
Ψ_s (10^{-1})
1.610
1.605
1.600
$N_\vartheta = 20$
$N_\varkappa = 20$
exact value
64
40
32
24
20

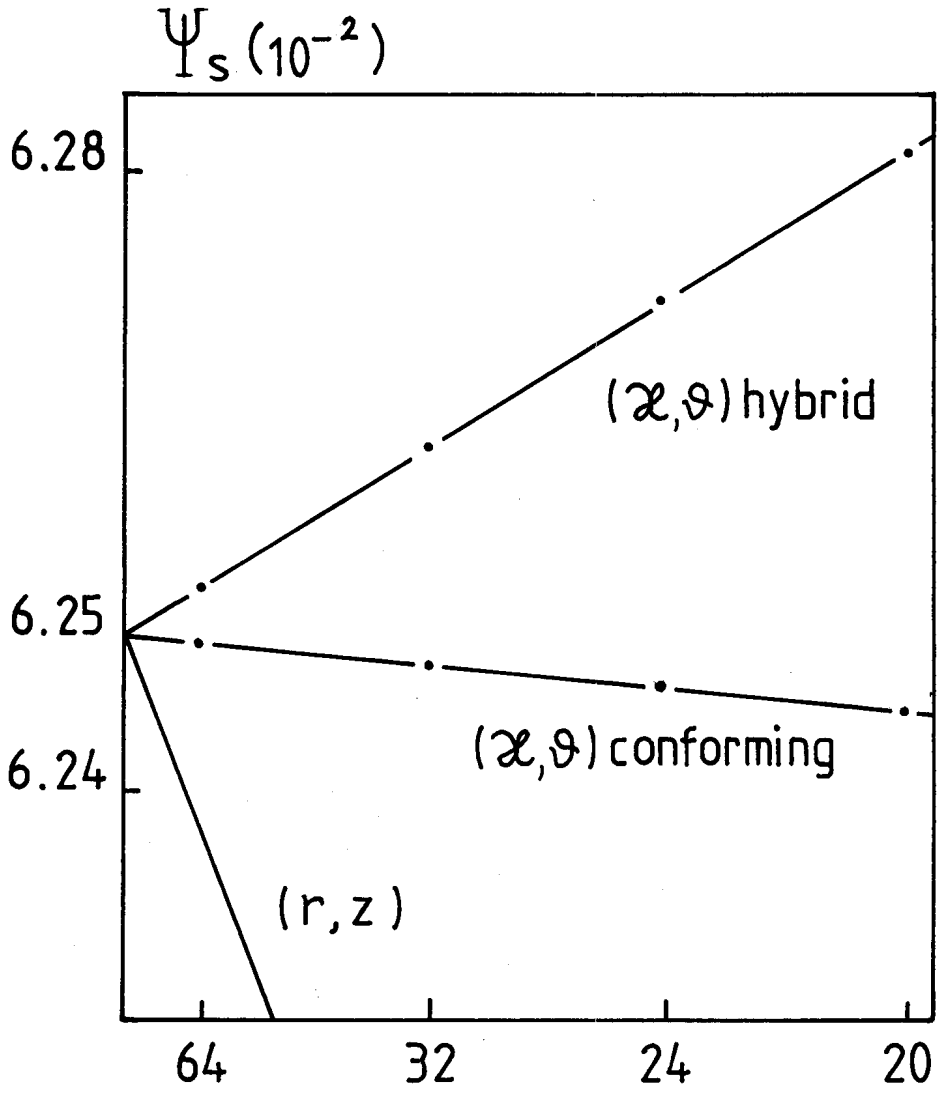
$\Psi_s\,(10^{-2})$
6.28
6.25
6.24
$(\mathcal{X},\vartheta)$ hybrid
$(\mathcal{X},\vartheta)$ conforming
(r, z)
64
32
24
20

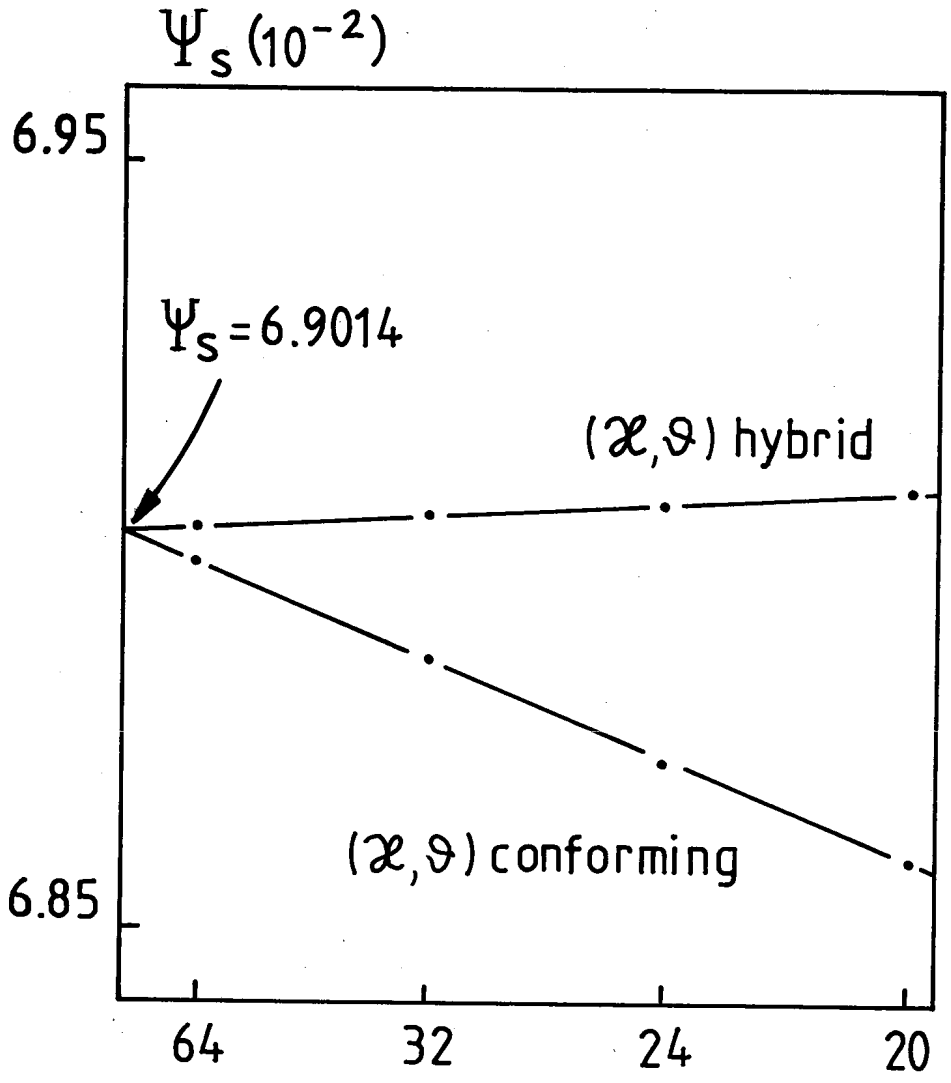
$\Psi_s\,(10^{-2})$
6.95
6.85
$\Psi_s = 6.9014$
$(\mathcal{X},\vartheta)$ hybrid
$(\mathcal{X},\vartheta)$ conforming
64
32
24
20

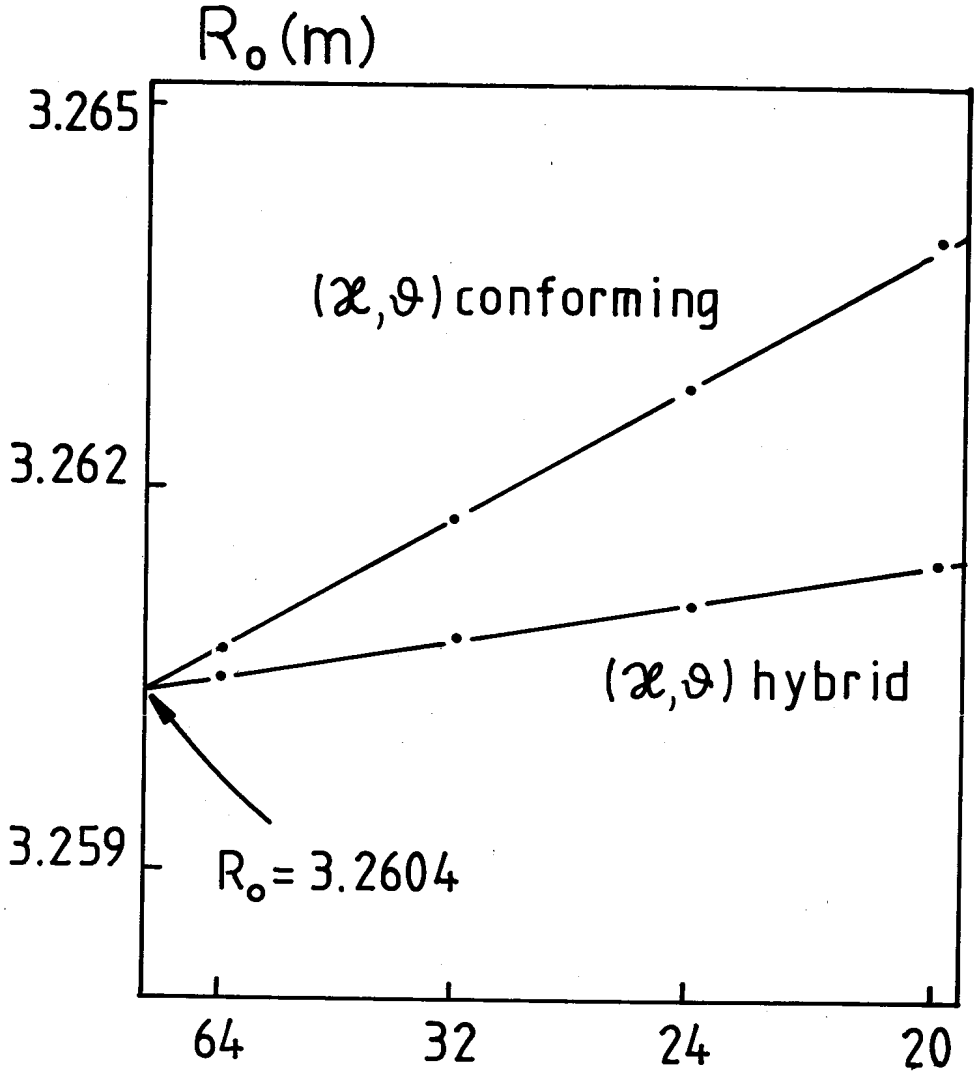
$R_o\,(m)$
3.265
3.262
3.259
$(\mathcal{X},\vartheta)$ conforming
$(\mathcal{X},\vartheta)$ hybrid
$R_o = 3.2604$
64
32
24
20